Helical γ-Peptide Foldamers as Dual Inhibitors of Amyloid-β Peptide and Islet Amyloid Polypeptide Oligomerization and Fibrillization

Julia Kaffy, Corentin Berardet, Loïc Mathieu, Baptiste Legrand, Myriam Taverna, Frédéric Halgand, Guillaume van Der Rest, Ludovic Maillard, Sandrine Ongeri

Chemistry
A European
Journal

Chemistry Europe
European Chemical Societies Publishing

Accepted Article

Title: Helical γ-peptide foldamers as dual inhibitors of amyloid-β peptide and islet amyloid polypeptide oligomerization and fibrillization

Authors: Sandrine Ongeri, Julia Kaffy, Corentin Berardet, Loïc Mathieu, Baptiste Legrand, Myriam Taverna, Frédéric Halgand, Guillaume Van Der Rest, and Ludovic Thierry Maillard

To be cited as: *Chem. Eur. J.* 10.1002/chem.202001716

Link to VoR: https://doi.org/10.1002/chem.202001716

WILEY-VCH

10.1002/chem.202001716

FULL PAPER

WILEY-VCH

Helical γ-peptide foldamers as dual inhibitors of amyloid-β peptide and islet amyloid polypeptide oligomerization and fibrillization

Julia Kaffy,*[a] Corentin Berardet,[a,b] Loïc Mathieu,[c] Baptiste Legrand,[c] Myriam Taverna,[b,e] Frédéric Halgand,[d] Guillaume Van Der Rest,[d] Ludovic T. Maillard,*[c] Sandrine Ongeri*[a]

[a] Dr. J. Kaffy, Dr. C. Berardet, Prof. S. Ongeri
Université Paris-Saclay, CNRS, BioCIS, 92290 Châtenay-Malabry, France
E-mail: julia.kaffy@universite-paris-saclay.fr
E-mail: sandrine.ongeri@universite-paris-saclay.fr

[b] Dr. C. Berardet, Prof. M. Taverna
Université Paris Saclay, CNRS, Institut Galien de Paris Sud, 92290 Châtenay-Malabry, France

[c] Dr L. Mathieu, Dr. B. Legrand, Dr L. T. Maillard
Institut des Biomolécules Max Mousseron, UMR 5247, CNRS, Universités Montpellier I et II, UFR des Sciences Pharmaceutiques et Biologiques, 15 Avenue Charles Flahault, 34093 Montpellier Cedex 5, France
E-mail: ludovic.maillard@umontpellier.fr

[d] Dr F. Halgand, Prof. G. Van Der Rest
Université Paris-Saclay, CNRS, Institut de Chimie Physique, 91405, Orsay, France

[e] Prof. M. Taverna
Institut universitaire de France

Supporting information for this article is given via a link at the end of the document

Abstract: Type 2 diabetes (T2D) and Alzheimer's disease (AD) belong to the 10 deadliest diseases and are sorely lacking in effective treatments. Both pathologies are part of the degenerative disorders named amyloidoses, involving the misfolding and the aggregation of amyloid peptides; hIAPP for T2D and $A\beta_{1-42}$ for AD. While hIAPP and $A\beta_{1-42}$ inhibitors have been essentially designed to target β-sheet rich structures composing the toxic amyloid oligomers and fibrils of these peptides, the strategy aiming at trapping the non-toxic monomers in their helical native conformation has been rarely explored. We report herein the first example of helical foldamers as dual inhibitors of hIAPP and $A\beta_{1-42}$ aggregation and able to preserve the monomeric species of both amyloid peptides. A foldamer composed of 4-amino(methyl)-1,3-thiazole-5-carboxylic acid (ATC) units, adopting a 9-helix structure reminiscent of 3_{10} helix, was remarkable as demonstrated by biophysical assays combining Thioflavin-T fluorescence, transmission electronic microscopy, capillary electrophoresis and mass spectrometry

Introduction

Type 2 diabetes (T2D) is a major public health issue, affecting nearly 400 million people in the world.[1] Alzheimer's disease (AD) is also of major concern with approximately 47 million people worldwide living with AD, number that is expected to reach 75 million by 2030.[2] At first glance, the two diseases appear to be completely distinct. However, clinical studies suggest that they are linked as they both involve impaired glucose homeostasis and altered brain function. Also T2D might be a risk factor for AD.[3–5] Insulin resistance, insulin degrading enzyme deficiency, oxidative stress are some of the common pathological conditions found in T2D and AD.[6–8] Furthermore, they both belong to a group of degenerative disorders called amyloidoses owing to the misfolding and the aggregation of amyloid proteins, namely amyloid-β peptide ($A\beta_{1-42}$) in the case of AD and human islet amyloid polypeptide (hIAPP) in the case of T2D.[9] $A\beta_{1-42}$ and hIAPP aggregates share structural characteristics such as highly ordered cross-β structures.[10] Emerging evidence supports the hypothesis that, in addition to the pathogenic self-assemblies, cross-amyloid interactions between $A\beta_{1-42}$ and hIAPP may also play a critical role in protein aggregation.[11,12] These observations led to a very recent interest for finding dual inhibitors of $A\beta_{1-42}$ and hIAPP.[13] Most of the modulators of $A\beta_{1-42}$ or hIAPP aggregation are designed to interact with the peptides in their β-sheet conformation and target the late fibrillar species. Indeed, they are mainly built on a planar aromatic scaffold such as the polyphenols resveratrol, epigallocatechin-3-gallate and curcumin, for which the β-sheet structures represent the major macromolecular target.[13–16] It is now admitted that preventing also the presence of soluble transient oligomers of $A\beta_{1-42}$ and hIAPP, that precede fibril formation, is crucial because they are highly toxic species and constitute a major cause of neurons and pancreatic islet cells death respectively.[17–19] Several small molecules such as polycyclic and polyphenols[14–16] or peptide derivatives[20–24] have been reported to target these oligomers. However, the aggregation process generates metastable species (dimer, small and larger oligomers), assumed to be unevenly toxic but that are inherently difficult to isolate and therefore to characterize. Furthermore, most of these species contain some β-sheet elements to different degrees but are nevertheless similar making difficult to selectively target one particular species. As the monomer forms of $A\beta_{1-42}$ and hIAPP are non-toxic and more easily cleared by enzymatic degradation, the strategy aiming to preserve them is of particular interest. Some of us recently demonstrated that peptides derivatives mimicking β-hairpin structures designed to bind small β-sheet oligomers were able to preserve $A\beta_{1-42}$ monomers.[21,22] An alternative strategy to trap $A\beta_{1-42}$ and hIAPP into their non-toxic monomeric forms would be to target their native form or their α-helix conformation before they switch to β-sheet structures that starts the aggregation process. However, only very few examples of ligands designed to interact with these amyloid peptides in their α-helical conformation support this hypothesis.[25–34] In this context, foldamer science[35–38] has

recently provided original solutions to modulate the kinetic pathway of amyloids. As a first exemple, the group of Miranker has recently reported that oligopyridine and oligoquinoline amides as α helical protein mimetic scaffolds may interfere with the early steps of folding of both $A\beta_{1-42}$ [26,28,30,31] and hIAPP[32–34] peptides by sequestering the helix-rich monomers. Similarly, the group of Bourgault has obtained interesting preliminary results with 2,5-diarylated thiophenes able to modulate hIAPP fibrillization.[39]

Based on helix-coil theory, 3_{10} helices have been proposed as probable intermediates in the conversion of α-helix to β-sheet during the $A\beta_{1-40}$ and hIAPP amyloidogenesis.[40,41] The reason for this suggestion is that there is a lower entropy penalty for closing the loop necessary for the formation of hydrogen bonds i → i + 3 versus i → i + 4. We hypothesized that targeting these species might interfere with self-association of both the amyloid proteins and prevent or delay aggregation. Over the last years, one of us explored a class of constrained heterocyclic γ-amino acids composed of 4-amino(methyl)-1,3-thiazole-5-carboxylic acids, named ATC (Fig. 1a). Interestingly, ATC foldamers showed high propensity to adopt a 9-helix structure[42] reminiscent of 3_{10} helix. Figure 1b is showing an overlay of 3_{10} helix and ATC foldamers backbones. First, the helical radius (2.0 Å) is similar to those of 3_{10} helix (1.9 Å), and the pitch is exactly double (12.0 Å vs 6.0 Å). Secondly, the lateral chains are distributed along three projection axes defining three distinct faces over the γ-peptide backbone. The substituents represented by red spheres in the γ position of the ATC (*i, i+4*) and on the thiazole ring of the ATC (*i+1*) are aligned on the same side of the helix in a manner almost similar to a canonical 3_{10} helix (orange spheres). Beside, the structure of the γ-peptide backbone showed low dependency on the nature of the substituents.[43] Thus, we hypothesized that by carefully selecting the side chains, the ATC foldamer scaffold could target a transient helical state of 3_{10} which is assumed at the first stages of the inter-conversion of the α-helix into β-sheet. We report herein our efforts to identify ATC foldamers disrupting the aggregation process occurring with $A\beta_{1-42}$ or hIAPP. By combining Thioflavin-T (Tht) kinetic assays, transmission electron microscopy (TEM), capillary electrophoresis (CE) and native mass spectrometry (MS) experiments, we identified a series of cationic foldamers as potent inhibitors of $A\beta_{1-42}$ and hIAPP aggregation (Fig. 1).

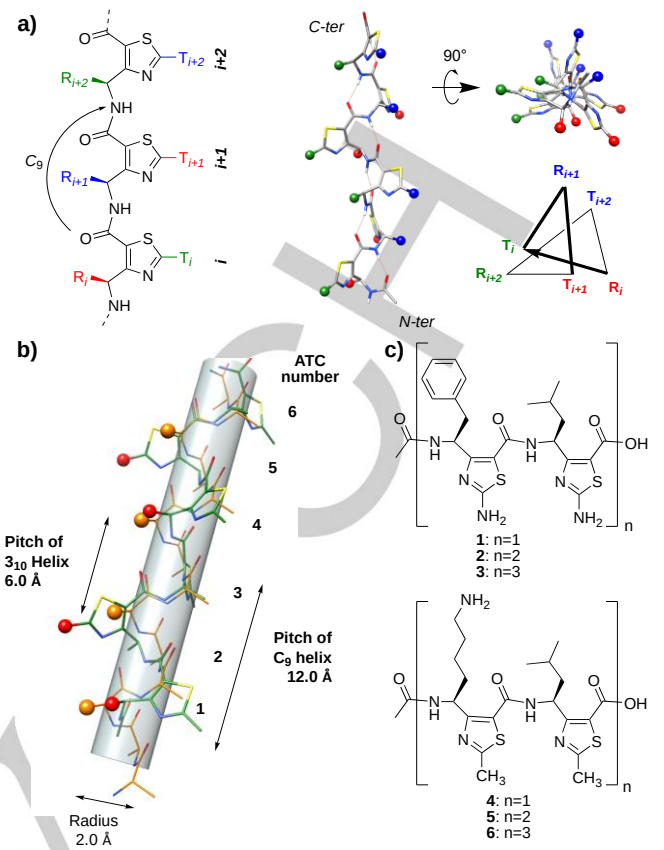

Figure 1. a) Helical topology of ATC foldamers showing the positions of thiazole substituents (T) and γ-side chains (R). b) Superimposition of a canonical 3_{10} helix (orange) and ATC foldamer (green). Spheres indicate the projection of the side chains along one face of the 3_{10} helix (orange spheres) and of the ATC foldamer (red sphere). c) Sequences of designed ATC foldamers.

Results and Discussion

Design, synthesis and structural characterization

We have prepared two series of foldamers displaying two to six ATC units. In a first series, γ-peptides **1**, **2**, **3** (2-, 4-, 6-ATC respectively) were flanked with hydrophobic substituents, *i.e*. *i*so-butyl and benzyl (Fig. 1c). Aromatic groups were introduced to specifically recognize phenylalanine residues which have been documented to play a key role in $A\beta_{1-42}$ and hIAPP amyloidogenic sequences ($_{16}$KLVFF$_{20}$[44–46] and $_{22}$NFGAIL$_{27}$[47,48] respectively). Amino groups at position 2 of the thiazole rings were expected to enhance the solubility as well to promote hydrogen bonds with the amyloids. Considering the second series, we assumed that introduction of cationic aminobutyl side chains on the foldamers **4**-**6** (2-, 4-, 6-ATC respectively, Fig. 1c) may likely establish electrostatic interactions with the negatively charged residues in the peptidic sequence of $A\beta_{1-42}$ ($E_{3\text{-}11\text{-}22}$, $D_{1\text{-}7\text{-}23}$ and A_{42}). Recently, we[21–24] and Hamilton[31] have independently recognized such a favorable effect of cationic amines to antagonize $A\beta_{1-42}$ amyloidogenesis.

The synthesis and the folding of compounds **4**, **5**, **6** were already reported.[42,49] They all adopt a right-handed helical shape in water from pH 3 to pH 11 at room temperature. The synthesis of foldamers **1**, **2** and **3** is shown in scheme 1. *N*-Fmoc-Phe-OH and *N*-Fmoc-Leu-OH were engaged in a cross-Claisen condensation to lead the β-ketoester **7a** and **7b** respectively. Monohalogenations were done using NBS and $Mg(ClO_4)_2$ as catalyst.[50] The resulting

α-bromo-β-ketoesters **8a** and **8b** were reacted with thiourea to lead to the fully protected intermediates **9a** and **9b**. Quantitative deprotection of the dimethylallyl esters were carried out with 3 mol% $Pd(PPh_3)_4$ and phenylsilane (Scheme 1a). The γ-peptides **1**-**3** were then prepared by solid-phase elongation of the *N*-Fmoc protected γ-amino acids **10a** and **10b** on chlorotrityl resin using EDCI and HOBt as coupling reagents. Finally, the terminal amine functions were acetylated then the peptides were released from the solid-support by TFA 5% in DCM. RP-HPLC purification led to foldamers **1**, **2** and **3** in 53%, 33% and 15% yield respectively (Scheme 1b). Structural studies of **1**, **2**, **3** were conducted in CD_3OH due to rather poor solubility in water at concentrations suitable for NMR experiments. The NMR signals of **1**, **2** and **3** were well dispersed. We noticed minor sets of resonances at the *C*-terminal part of the foldamers **2** and **3** (Fig. S3 b), c), SI) since this extremity is fraying probably due to the absence of hydrogen bond involving the terminal carboxylic acid function. The sequential assignment was based on the strong NH(*i*)/ $^{\gamma}$CH(*i*-1) NOE correlations classically observed on the ROESY/NOESY spectra of helical foldamers. The strong NH deshielding (> 9 ppm) (Table S1, S2, S3, SI) as well as ^3J(NH,$^{\gamma}$CH) values < 6 Hz (Table S4, SI) which have been recognized as a structural marker related to the formation of a C_9 hydrogen-bonding pattern[51] were also in agreement with a global helix structure. The C_9-helical behavior of the foldamers was confirmed by circular dichroism. CD spectra were recorded at rt and 200 µM concentration in MeOH. With a minimum at 232 nm and a maximum at 264 nm assigned respectively to the n-π* transitions of the amide chromophore, and to the thiazole core, the CD signatures of **2**-**3** in methanol were similar to those of **5**-**6** (Fig. S4, SI).[42] Some differences in the signal intensity and signature were observed for the **1** and **4**, suggesting a partial unfolding for the shortest molecules.

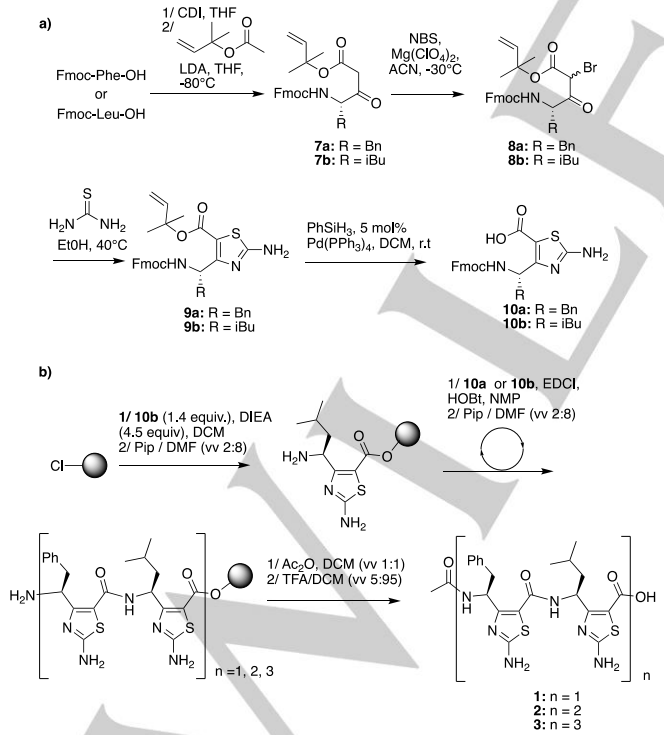

Scheme 1. Synthesis of compounds **1**-**3**. a) ATC building-blocks synthesis. b) SPPS ATC elongation.

Inhibition of $A\beta_{1-42}$ and hIAPP fibrillization

ThT-fluorescence experiments

The ability of foldamers **1**-**6** to interact with $A\beta_{1-42}$ and hIAPP fibril formation was first investigated using the *in vitro* Thioflavin-T (Tht) fluorescence assay. ThT is the standard dye used to monitor the kinetics of aggregation of amyloid proteins because it fluoresces upon binding to β-sheet rich structures.[52] The fluorescence curves for $A\beta_{1-42}$ and hIAPP controls displayed the typical sigmoidal pattern, starting with an initial lag phase lasting around 3-5 h for $A\beta_{1-42}$ and 1 h for hIAPP, followed by a rapid polymerization phase ending by a plateau reached after 10-15 h for $A\beta_{1-42}$ and 5 h for hIAPP. Each compound was tested at three different foldamer/amyloid peptide ratios, *i.e*. from 10/1, 1/1 to 0.1/1. Two parameters were gathered from the fluorescence curves analysis: (1) $t_{1/2}$, defined as the time at which fluorescence has reached half of its maximal value and gives insight on the kinetics of the aggregation process and (2) F, the fluorescence intensity at the plateau, which is, in a first approximation, related to the amount of fibrillar material formed.

Regarding the fibrillization of $A\beta_{1-42}$, **1** and **2** were inactive and **3** self-associated at 100 µM thus precluding any evaluation of its activity (Table 1 and Fig. S5, SI). By contrast, a significant foldamer size- and dose-dependent inhibitory effect was observed with the second series **4**-**6** (Table 1, Fig. 2a and S5, SI). 2-ATC foldamer **4** showed a modest activity on the fibrillization at 10/1 and 1/1 ratios of **4**/$A\beta_{1-42}$ while 4-ATC foldamer **5** exhibited a higher inhibitory effect. At a 10-fold excess, the fibrillization was strongly delayed by 127%. At a 1/1 ratio and despite a moderate effect on the fluorescence at the steady state (ΔF = -15%), the $t_{1/2}$ value was further increased by 50 % compared to the control experiment. No effect was detected at a substochiometric 0.1/1 ratio. The most significant activity on $A\beta_{1-42}$ aggregation was obtained with the longer 6-ATC foldamer **6** for which a complete inhibition of the fibrillization was reached at a 10/1 ratio (Fig. 2a). At a 1/1 ratio, the activity on both the kinetics ($\Delta t_{1/2}$ = 130 %) and the fluorescence plateau (ΔF = -40%) was as high as that of the 4-ATC compound **5** at a 10/1 ratio. Remarkably, an inhibitory activity was still observed at the low 0.1/1 ratio of **6**/$A\beta_{1-42}$ ($\Delta t_{1/2}$ = 55 %; ΔF = -19%).

Foldamers **1**-**2** were mainly inactive on the aggregation of hIAPP and **3** self-associated at 50 µM thus precluding any evaluation of its activity (Table 1 and Fig. S6, SI) while foldamers **4**-**6** displayed a foldamer size- and dose-dependent inhibitory effect on the fibrillization of hIAPP (Table 1, Fig. 2b and S6, SI). At a 10-fold excess, 2-ATC and 4-ATC compounds, **4** and **5** showed a delay in the kinetics of aggregation ($\Delta t_{1/2}$ = 59 and 159 % respectively). At a lower ratio, they were almost inactive. The most significant activity was once again obtained with 6-ATC foldamer **6**. At a 10/1 ratio, $\Delta t_{1/2}$ > 400 % and the plateau was decreased by more than 60 % (Fig. 2b). The effect was only partially maintained at a 1/1 ratio ($\Delta t_{1/2}$ = +21% and no effect on F) and completely suppressed at a 0.1/1 ratio. In 2013, Miranker *et al.*[32] demonstrated that, oligoquinoline helical compounds have a stronger inhibitory activity on the aggregation of hIAPP in the presence of phospholipids bilayers. One reason would be that helical species of hIAPP are more populated when the amyloid is mixed with membrane models. Contrariwise, small aromatic planar inhibitors such as resveratrol and acid fuchsin display lower activity in the presence of liposomes in connection with a probable interaction with β-sheet species. In the case of 6-ATC foldamer **6**, the anti-fibrillization activity was significantly reduced when 1mg/mL of large unilamelar vesicles (LUV) were added to the Tht/hIAPP

10.1002/chem.202001716

mixture. We cannot totally exclude that the β-sheet forms of hIAPP are targeted by **6**, however we rather believe that cationic foldamer **6** is trapped by the highly anionic liposomes, preventing its interaction with hIAPP species.

Interestingly, thanks to its three amino groups, foldamer **6** was totally soluble in aqueous media and its activity on $A\beta_{1-42}$ and hIAPP fibrillization was maintained even in the absence of DMSO as cosolvent (Table 1, Fig. S5 and S6, SI). This result is of particular interest to pursue biological applications.

Table 1. Effects of compounds 1-6 on $A\beta_{1-42}$ and hIAPP fibrillization assessed by ThT-fluorescence spectroscopy at 10/1, 1/1 and 0.1/1 ratios of foldamer/amyloid.

	Effects on $A\beta_{1-42}$		**Effects on hIAPP**	
Compounds (compound/amyloid ratio)[a]	$t_{½}$ increase (%)[b]	F decrease (%)[c]	$t_{½}$ increase/ decrease (%)[b]	F decrease (%)[c]
1 10/1	ne[d]	ne	+7±1	–40±24
1 1/1	ne	ne	ne[d]	ne
1 0.1/1	ne	ne	ne	ne
2 10/1, 1/1, 0.1/1	ne	ne	ne	ne
3 10/1[e]	nd[f]	nd	nd	nd
3 1/1	ne	ne	–44±7	ne
3 0.1/1	ne	ne	ne	ne
4 10/1	+21±1	–35±5	+59±28	ne
4 1/1	ne	–29±8	+17±11	ne
4 0.1/1	ne	ne	ne	ne
5 10/1	**+127±13**	**–39±3**	**+159±50**	ne
5 1/1	**+50±1**	–15±8	ne	ne
5 0.1/1	ne	ne	ne	ne
6 10/1	**NA**[g]	**–92±2**	**+404±45**	**–62±8**
6 1/1	**+130±6**	**–40±4**	**+21±12**	ne
6 0.1/1	**+55±5**	–19±8	ne	ne
6 (water) 10/1	**NA**	**–84±2**	**+490±30**	**–67±1**
6 (water) 1/1	**+169±17**	**–57±6**	ne	ne

Parameters are expressed as mean ± SE, n=3. [a] Unless otherwise indicated, compounds were dissolved in DMSO; the final concentration kept constant at 0.5 % (v) and 3 % for respectively $A\beta_{1-42}$ and hIAPP. The concentration of $A\beta_{1-42}$ was 10 μM while the concentration of hIAPP was 5μM [b] See supporting information for the calculation of the $t_{1/2}$ increase/decrease. [c] See supporting information for the calculation of the F decrease. [d] ne = no effect, [e] compound **3** self-aggregates at 100 and 50μM, [f] nd = not determined, [g] NA = no aggregation.

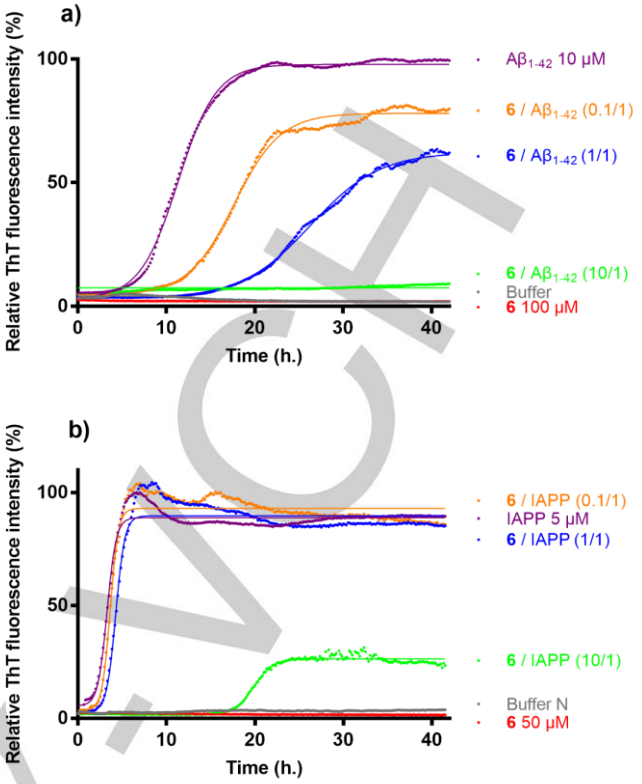

Figure 2. Kinetics of amyloid fibril formation followed by ThT fluorescence. Representative curves showing aggregation of ; **a)** $A\beta_{1-42}$ (10 μM) at a foldamer **6**/amyloid peptide ratio = 0/1, 0.1/1, 1/1 and 10/1; **b)** hIAPP (5 μM) at a foldamer **6**/amyloid peptide ratio = 0/1, 0.1/1, 1/1 and 10/1.

Transmission electron microscopy experiments

Transmission electron microscopy (TEM) analyses were then performed on 6-ATC foldamer **6** to explore its impact on $A\beta_{1-42}$ and hIAPP fibrillar material. Images were recorded at 1/1 and 10/1 ratios of **6**/amyloid peptide after 42 h or 17 h of incubation which correspond to maximum aggregation of $A\beta_{1-42}$ and hIAPP respectively, in the ThT assays. In the control sample, $A\beta_{1-42}$ formed a typical very dense network of long fibers (Fig. 3a). At an equimolar ratio of foldamer **6**, the amount of fibrillar material remained significantly less important than that of the control grid, the network was moderately dense and short fibrils entangled in large aggregates were observed (Fig. 3b). At a 10/1 ratio of **6**/$A\beta_{1-42}$ (Fig. 3c) only shorter, thinner and very scarce fibers, compared with those observed in the control grid were visible. For hIAPP, the control sample displayed a typical morphology consisting of an extremely dense network of long and tangled fibers (Fig. 3d). At a 1/1 ratio of **6**/hIAPP, the network displayed a comparable morphology than in the control grid (Fig. 3e). However, at a 10/1 ratio, only very short, straight and scarce fibers were observed (Fig. 3f). Thus, these results are in accordance with the ThT-fluorescence data and confirm the efficiency of foldamer **6** to disrupt the fibrillization process of both $A\beta_{1-42}$ and hIAPP amyloid peptides.

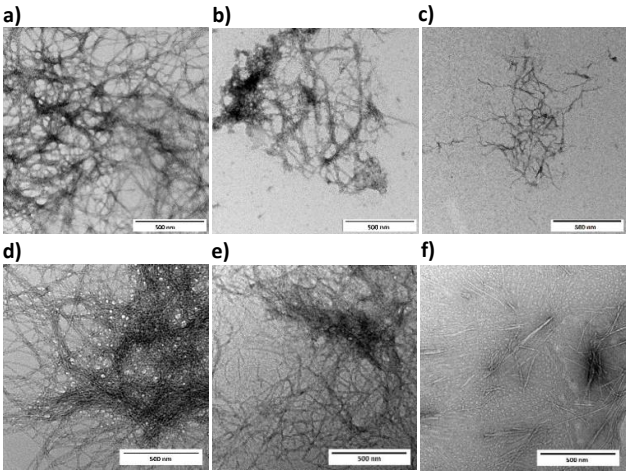

Figure 3. Effect of foldamer **6** on the fibril formation of $A\beta_{1-42}$ and hIAPP visualized by TEM (Scale bars, 500 nm). Negatively stained images recorded after 42 h of incubation for 10 µM $A\beta_{1-42}$ (**a, b, c**) and 17 h of incubation for 5 µM hIAPP (**d, e, f**) in 10 mM Tris·HCl and 100 mM NaCl at pH 7.4. **b), e)** Experiments performed at a 1/1 ratio of **6**/amyloid peptides. **c), f)** Experiments performed at a 10/1 ratio of **6**/amyloid peptides.

Activity on $A\beta_{1-42}$ and IAPP oligomerization by capillary electrophoresis experiments.

We next evaluated the effect of foldamer **6** on the oligomerization process of $A\beta_{1-42}$ and hIAPP peptides using capillary electrophoresis (CE). Some of us developed this technique for monitoring soluble species formed during the early $A\beta_{1-42}$[21–23,53] and hIAPP[54,55] aggregation processes. The typical electrophoretic profile over time for the $A\beta_{1-42}$ control sample is shown in figure 4a. At the beginning of the kinetics, the monomer ES was the major visible species associated with a very small amount of small oligomers ES' (dimers to tetramers).[53] The monomer contribution decreased steadily to totally disappear after 10 h (Fig. 4a) and some insoluble aggregates (spikes) appeared from 5 h (visible in Fig. S7, SI). Although large soluble aggregates (LS) are not easily detected with the chosen scale of this figure a small amount of these species can be detected by extending the Y axis scale (Fig. S7, SI). Nevertheless, the peak area of this LS fraction represented as a very broad peak is hardly reproducible and vary quite significantly form one experiment to another.[21–23,53] Conversely, foldamer **6** greatly delayed the oligomerization process. At a 1/1 ratio of **6**/$A\beta_{1-42}$ (Fig. 4c) the monomer was dramatically stabilized and 70 % of the ES species remaining visible until 20 h (see peak area of the monomer (ES) related to its maximum peak area in the control sample, Fig. 4d). Small ES' species remained very low. Interestingly, larger soluble aggregated species (LS peak[21–23,53]) described as toxic forms of $A\beta_{1-42}$ were not produced (Fig. S8, SI). By contrast, spikes attributed to unspecific insoluble aggregates appeared after 1 h and their quantity was noticeable from 5 h but almost disappeared at 20 h. Also to note, a large peak migrating before the electroosmotic flow (EOF) one was observed at the beginning of the kinetics (also visible in the electrophoretic profile of **6** control, Fig. 4b). We hypothesize that this peak was composed of associated forms of foldamer **6** trapping eventually $A\beta_{1-42}$ monomers. These associated forms get dissociated after 5 h leading to free compound **6** and $A\beta_{1-42}$ monomer. Overall, CE results demonstrate that foldamer **6** is able to greatly delay the oligomerization process of $A\beta_{1-42}$ even at the low 1/1 ratio, by strongly stabilizing $A\beta_{1-42}$ monomer, described as non-toxic species, and by preventing the presence of large soluble aggregates

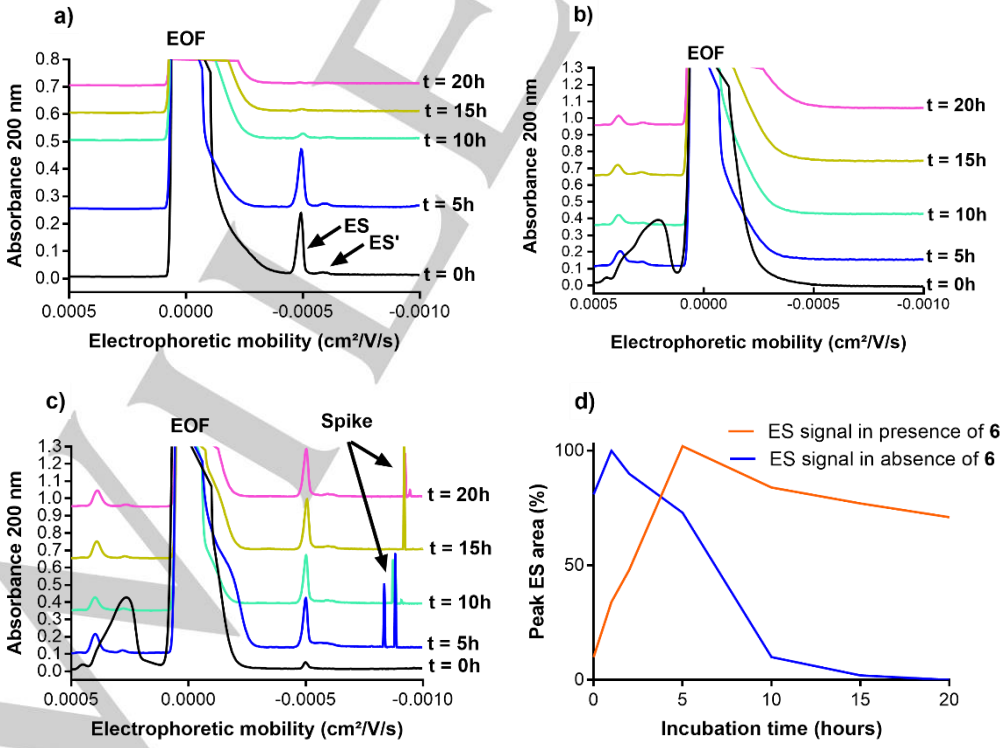

Figure 4. Electrophoretic profiles over time (0 to 20h) of control samples of $A\beta_{1-42}$ (100 µM, **a**) and **6** (100 µM, **b**). EOF: electroosmotic flow; ES: monomer of $A\beta_{1-42}$; ES': small oligomers. **c)** Electrophoretic profile over time (0 to 20 h) of $A\beta_{1-42}$ peptide (100 µM) incubated with **6** (100 µM). **d)** Evolution of the $A\beta_{1-42}$ monomer area (ES) over time in the absence or in the presence of **6** (1/1 ratio of **6**/$A\beta_{1-42}$) relative to $A\beta_{1-42}$ monomer area at t = 1 h.

In the case of hIAPP, three groups of soluble species were formed during the 20 hours aggregation process, as we previously reported.[54] Peak 3 was attributed to monomer species which are co-populated with a very small amount of dimers and trimers, whereas we demonstrated that peaks 1 and 2 were mainly composed of large oligomeric species with a mass higher than 100 kDa, corresponding to species of about 25-mers.[54] The electrophoretic profile of hIAPP control showed that the amount of monomer decreased steadily to almost disappear after 5h (Fig. 5a). Concomitantly, the quantity of soluble oligomers (peak 2) regularly increased from 0 to 20 h. The amount of oligomers migrating in peak 1 could not be evaluated as these species comigrated with the EOF. By comparison, foldamer **6** at 1/1 ratio significantly stabilized the hIAPP monomer forms (peak 3) up to 15 h (Fig. 5c). The kinetics of decrease of the monomer species with and without **6** is shown in figure 5d. It appeared that after 10 h incubation, more than 60 % of hIAPP monomer was maintained in the presence of compound **6** whereas the corresponding peak almost disappeared in the hIAPP control. This observation indicates that compound **6** strongly delays hIAPP oligomerization by essentially stabilizing the monomers of hIAPP.

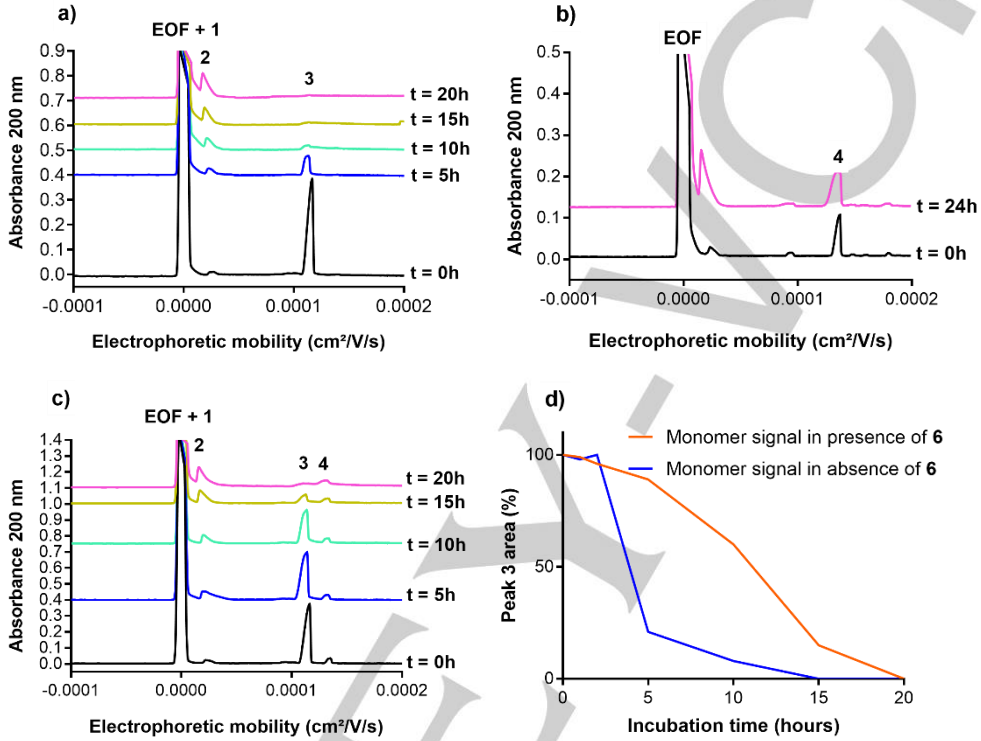

Figure 5. Electrophoretic profiles over time (0 to 20h) of control samples of **a)** hIAPP (100 µM) and **b) 6** (100 µM). EOF: electroosmotic flow; Peaks 1 and 2: large oligomer species; Peak 3: monomer of hIAPP; Peak 4: foldamer **6**. **c)** Electrophoretic profile over time (0 to 20 h) of hIAPP peptide (100 µM) incubated with **6** (100 µM). **d)** Evolution of the hIAPP monomer area (peak 3) over time in the absence or presence of **6** (1/1 ratio of **6**/hIAPP) relative to hIAPP monomer peak area at t = 0 h.

Native mass spectrometry experiments

Mass spectrometry (MS) and ion mobility spectrometry-mass spectrometry (IMS-MS) have been recently proposed for monitoring hIAPP species formed within the oligomerization process as well as for probing mechanisms of inhibition of hIAPP fibril formation.[55–60] Using the same buffer conditions as for CE experiments (50 µM hIAPP, 50 mM AA, pH 3.7 at room temperature) the MS spectrum showed the classically observed dynamic set of hIAPP species, mostly monomer to hexamer species in multiple charge states, (Fig. 6a, b). In the presence of **6** and whatever the **6**/hIAPP stoichiometry considered (1/1, 5/1 and 10/1), high mass oligomer species such as tetramers, pentamers, hexamers completely disappeared (Fig. 6c-e). At 5/1 and 10/1 ratios, the formation of dimers and trimers strongly decreased. The relative abundance of the oligomeric species was finally determined at 5 µM hIAPP because at 50 µM, we were confronted with detector saturation due to monomer signals. Large oligomers, *i.e.* tetramer, pentamer and hexamer forms were no longer detectable in these conditions. We could not totally exclude that a ten-fold dilution reduces the oligomeric order or simply induces the loss of low abundance species. However, the comparison we made remains valid. Considering all the charge states (CS), the abundance of dimer and trimer relative to the monomer decreases with the increase in concentration of **6** (Fig. 7a-b). Note here that peaks at *m/z* corresponding to the complex of hIAPP peptide with the foldamer **6** do not overlap with monomer or dimer of intact hIAPP. However, dimer of the intact hIAPP monomer could overlap with several charge states of the monomer such as +6 CS of the dimer with the +3 CS of the monomer. Such possibility has been checked and overlapped contributions of the different species for identical CS were found negligible. Thus, from both CE and MS experiments, we can conclude that the foldamer **6** dramatically slows down the fibrillization process not by stabilizing soluble oligomers species but rather by maintaining hIAPP in a native-like monomeric state. Furthermore, as direct evidence, the non-covalent 1:1, 2:1 and 3:1 complexes of **6** with the monomeric hIAPP peptide were detected (Fig. 6c, d, e). A determination of the K_d of these complexes using this titration experiment was attempted, but was not successful, presumably due to a low Kd or too strong gas phase dissociation of the complex. Nevertheless, the trend of an increase in the proportion of monomeric hIAPP/**6** complexes to monomeric hIAPP when the concentration of **6** is increased (Fig. 7c) points out towards a specific binding of these partners in the solution phase.

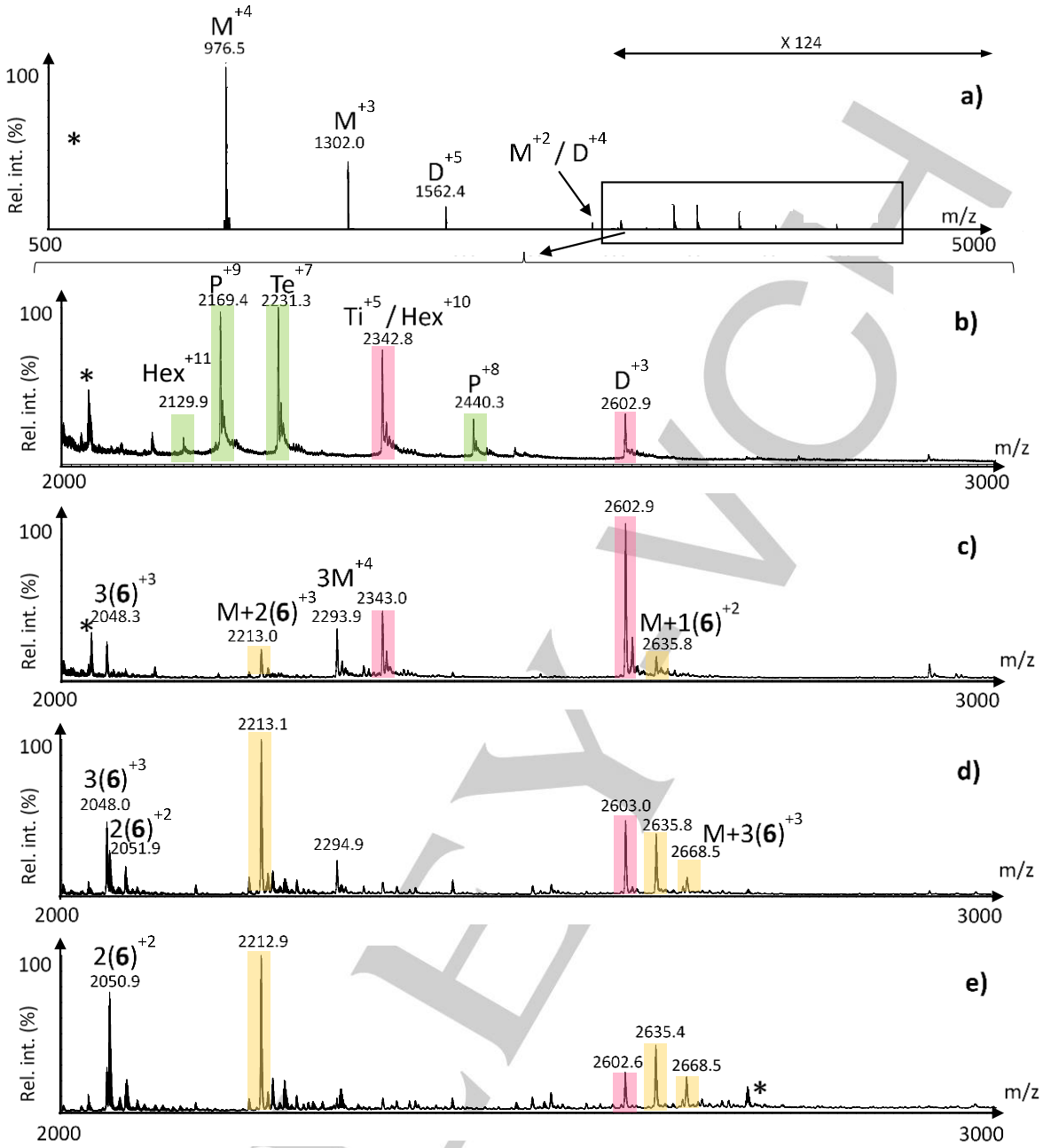

Figure 6. Mass spectra of hIAPP alone for the 500 – 5000 *m/z* range (**a**) and for the 2000 – 3000 *m/z* range (**b**); mass spectra of hIAPP for the 2000 – 3000 *m/z* range with the foldamer **6** at a 1/1 (**c**), 5/1 (**d**) and 10/1 (**e**) ratios of **6**/hIAPP. **Legends:** M= hIAPP monomer, (**6**) = foldamer **6**, D = hIAPP dimer, Ti = hIAPP trimer, Te = hIAPP tetramer, P = hIAPP pentamer, Hex = hIAPP hexamer; ***** = contaminant.

10.1002/chem.202001716

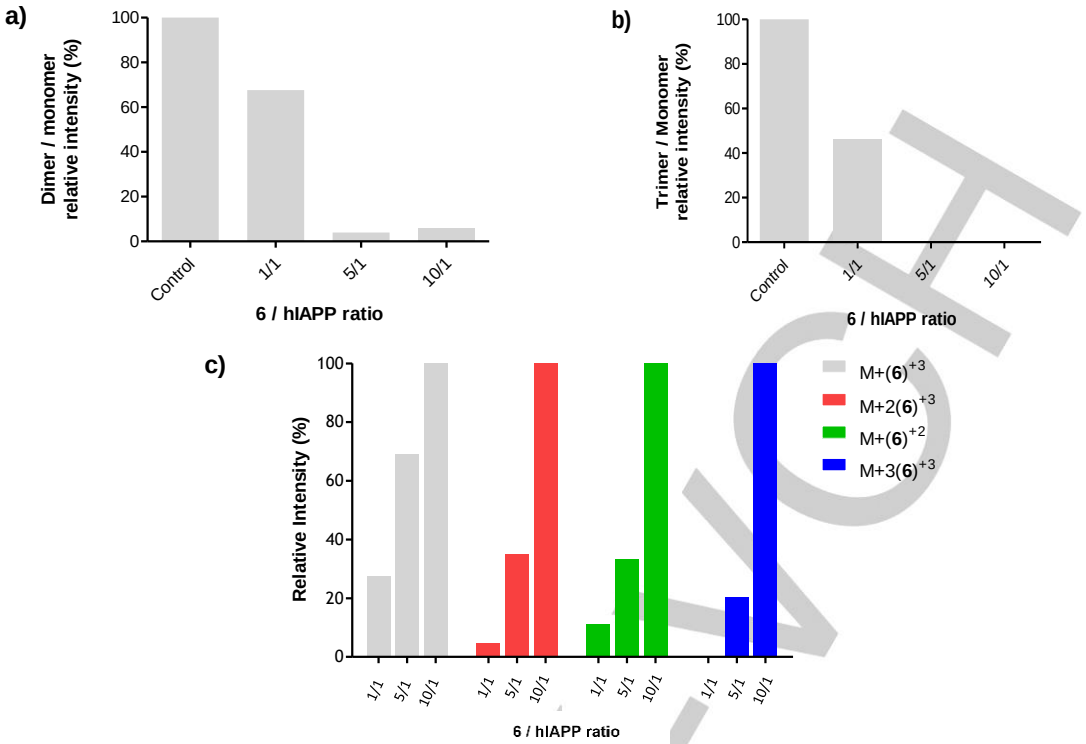

Figure 7. a-b) Ratios of dimer/monomer and trimer/monomer species of hIAPP calculated from the ESI-MS mass spectrum. **c)** Relative intensities of MS signals associated to the non-covalent 1:1, 2:1 and 3:1 complexes of **6** with the monomeric hIAPP peptide (M) at **6**/hIAPP ratios of 1/1, 5/1, 1

Conclusions

Chemical chaperone molecules that can stabilize the protein native structures, in order to prevent its misfolding into β-sheet rich species and inhibit self-assembly, have been considered as potential promising drug candidates in amyloidosis. Indeed, monomer forms of the amyloid proteins $A\beta_{1-42}$ and hIAPP are non-toxic and more easily cleared by enzymatic degradation. However, the amyloid precursors are intrinsically disordered proteins (IDPs), which makes structure-based drug design very complex. In such a context, peptide-based molecules and peptidomimetics represent an opportunity to create nano-scale, definable surfaces to bind protein interfaces.

In this work, we took advantage of an easy modulation of the ATC side chains to develop C9-helical foldamers to antagonize the aggregation process of $A\beta_{1-42}$ and hIAPP. Due to structural homologies with 3_{10} helices, which is a transient state assumed at the early steps of the inter-conversion of α-helix to β-sheet of amyloids, ATC foldamers were expected to disrupt the early steps of self-assembling by stabilizing peptides in their native conformation. In a first series, benzyl side chains were considered to target the phenylalanine rich amyloidogenic sequences of $A\beta_{1-42}$ and hIAPP in which aromatic π-π interactions have been suggested to play a crucial role in the aggregation process. In a second series, we introduced cationic substituents with the goal to increase the water solubility and possibly to establish electrostatic interactions with the negatively charged residues in $A\beta_{1-42}$. Combinations of biophysical techniques have been used to demonstrate the size and dose-dependent ability of ATC foldamers to inhibit the aggregation of $A\beta_{1-42}$ and hIAPP. In particular, thanks to our recently developed methods by CE and MS, the early steps of the self-assembling and the effect on the stabilization of the native monomer species could be investigated. While 2- and 4- ATC foldamers of both series have almost no or little effect on the aggregation processes, the water-soluble 6-ATC foldamer **6** was proven to dramatically modulate the aggregation process of both $A\beta_{1-42}$ and hIAPP. Surprisingly, the 6-ATC foldamer **3** having benzyl groups instead of aminoalkyl chains was not active. To our opinion, this cannot be explained by a decrease of affinity of the helical shape due to the simple replacement of these chains. We rather hypothesize that the strong propensity of foldamer **3** to self-associate as shown by the ThT experiments, might be due to its high hydrophobicity and π-stacking possibilities. This auto-aggregation excludes its availability to interact with monomers or small soluble species of amyloid proteins. Noticeably foldamer **6** dramatically alters the early oligomerization event of $A\beta_{1-42}$, even at 1/1 ratio. Remarkably, at a higher 10/1 ratio, it also showed a significant activity on hIAPP fibrillization. Its preference for $A\beta_{1-42}$ is probably related to the establishment of ionic interactions with the anionic residues and the acidic *C*-terminus (^{22}E, ^{23}D, ^{42}A), which are involved in the folding of $A\beta_{1-42}$.[20-23] hIAPP having no acidic residues, the stabilizing effect induced by **6** is less marked and possibly results from hydrophobic interactions mediated by *i*Bu groups and methyl-thiazole rings. However, possible ionic interaction between the acidic *C*-terminus of **6** and hIAPP ^{11}R, a key residue in the misfolding transition is feasible. Because of the inherent dynamic of $A\beta_{1-42}$ and hIAPP peptides, detailed characterization of molecular interaction events was precluded. We are aware that additional experiments could bring further information on the conformational state of the trapped monomers. CD experiments were attempted to validate the ability of **6** to stabilize helical conformations of $A\beta_{1-42}$ and hIAPP in buffer but the intense signal of **6**^{42} at the active concentration did not allow to appreciate the conformational transition of the amyloid even after substraction. Moreover, even at 10-fold lower concentration, the foldamer signal interfered with the classical CD curve of hIAPP peptide. The use of high resolution approaches such as NMR could be considered in a second

approach to obtain further mechanistic insights. Nevertheless, we demonstrated from native MS experiments that foldamer **6** is binding monomer species. Indeed, non-covalent foldamer **6**:hIAPP monomer complexes (1:1, 2:1 and 3:1) were unambiguously observed in MS spectra, while a decrease of oligomeric species (up to hexamer) was observed as the concentration of **6** increases. CE experiments confirmed that monomer species of $A\beta_{1-42}$ and hIAPP persist for a longer time in the presence of foldamer **6**.

ATC-based γ-peptide foldamers are promising scaffolds to target IDPs such as amyloid proteins. The versatile and robust synthetic pathway affords the possibility of pharmacomodulations to increase their ability to prevent amyloid proteins self-association. In particular, the nature of the side chains along the faces of the helical shape might be modulated in order to extend and adapt their use to selectively target other amyloid proteins.

Experimental Section

*Synthesis of foldamers **1**-**3***
The protocols of synthesis of **1**-**3** are given in Supporting Information.

Fluorescence-Detected ThT Binding Assay ($A\beta_{1-42}$).
$A\beta_{1-42}$ was purchased from American Peptide and ThT was obtained from Sigma. The peptide was dissolved in an aqueous 1% ammonia solution to a concentration of 1 mM and then, just prior to use, was diluted to 0.2 mM with 10 mM Tris-HCl and 100 mM NaCl buffer (pH 7.4). Stock solutions of foldamers were dissolved in DMSO or in water with the final concentration kept constant at 0.5% (v/v). ThT fluorescence was measured to evaluate the development of $A\beta_{1-42}$ fibrils over time using a fluorescence plate reader (Fluostar Optima, BMG labtech) with standard 96-well black microtiter plates (final volume in the wells of 200 µL). Experiments were started by adding the peptide (final $A\beta_{1-42}$ concentration equal to 10 µM) into a mixture containing 40 µM ThT in 10 mM Tris-HCl and 100 mM NaCl buffer (pH 7.4) with and without the foldamers at different concentrations (100, 10, 1 µM) at room temperature. The ThT fluorescence intensity of each sample (performed in duplicate or triplicate) was recorded with 440/485 nm excitation/emission filters set for 42 h performing a double orbital shaking of 10 s before the first cycle. The fluorescence assays were performed between 2 and 4 times on different days, with the same batch of peptide. The ability of compounds to inhibit $A\beta_{1-42}$ aggregation was assessed considering the time of the half-aggregation ($t_{1/2}$) and the intensity of the experimental fluorescence plateau (F), both values were obtained by fitting the obtained kinetic data to a Boltzmann sigmoidal curve using GraphPad Prism 5. The relative increase of $t_{1/2}$ is defined as the experimental $t_{1/2}$ in the presence of the tested compound relative to the one obtained without the compound and is evaluated as the following percentage: [$t_{1/2}$ (Aβ + compound) − $t_{1/2}$ (Aβ)] / $t_{1/2}$ (Aβ) × 100. The decrease of the experimental plateau is defined as the intensity of experimental fluorescence plateau observed with the tested compound relative to the value obtained without the compound and is evaluated as the following percentage: (FAβ + compound – FAβ) / FAβ × 100. The curves of the active (or self-aggregating) compounds are fitted to a Boltzmann sigmoidal model, normalized to the control experiment and represented in supporting information (Fig. S5, SI).

Fluorescence-Detected ThT Binding Assay (hIAPP).
hIAPP, purchased from Bachem, was dissolved in pure hexafluoro-isopropanol (HFIP) at a concentration of 1 mM and incubated for 1 hour at room temperature to dissolve any preformed aggregates. Next, HFIP was evaporated with dry nitrogen gas followed by vacuum desiccation for 3 hours. The resulting peptide film was then dissolved in DMSO to obtain stock solutions of hIAPP (0.2 mM). Stock solutions of foldamers were dissolved in DMSO or in water (10, 1 and 0.1 mM). The concentration of DMSO was kept constant at 3% (v/v) in the final volume of 200 µL. Thioflavin-T binding assays were used to measure the formation of fibrils over time. A plate reader (Fluostar Optima, BmgLabtech) and standard 96-wells flat-bottom black microtiter plates in combination with a 440 nm excitation and 485 nm emission filters were used. The ThT assay was started by adding 5 µL of a 0.2 mM hIAPP stock solution to a mixture of 10 µM ThT and 10 mM Tris/HCl, 100 mM NaCl at pH 7.4 containing 1 µL of stock solutions of foldamers. The concentration of IAPP was held constant at 5 µM and foldamers were added to yield foldamer/IAPP ratios of 10/1, 1/1 and 0.1/1. The ThT assays were performed in duplicate or triplicate and between 2 and 4 times on different days, with the same batch of peptide. The ability of compounds to inhibit IAPP aggregation was assessed considering the time of the half-aggregation ($t_{1/2}$) and the intensity of the experimental fluorescence plateau (F), both values were obtained by fitting the obtained kinetic data to a Boltzmann sigmoidal curve using GraphPad Prism 5. The relative increase (or decrease) of $t_{1/2}$ is defined as the experimental $t_{1/2}$ in the presence of the tested compound relative to the one obtained without the compound and is evaluated as the following percentage: [$t_{1/2}$ (hIAPP + compound) − $t_{1/2}$ (hIAPP)] / $t_{1/2}$ (hIAPP) × 100. The decrease of the experimental plateau is defined as the intensity of experimental fluorescence plateau observed with the tested compound relative to the value obtained without the compound and is evaluated as the following percentage: (FhIAPP + compound – FhIAPP) / FhIAPP × 100. The curves of the active (or self-aggregating) compounds are fitted to a Boltzmann sigmoidal model, normalized to the control experiment and represented in supporting information (Fig. S6, SI).

Transmission Electron Microscopy.
$A\beta_{1-42}$ experiments. Samples were prepared under the same conditions as those in the ThT-fluorescence assay except that Tht was not added. Aliquots of $A\beta_{1-42}$ (10 µM in 10 mM Tris-HCl and 100 mM NaCl, pH 7.4 in the presence and absence of foldamer **6**) were adsorbed onto 300-mesh carbon grids for 2 min, washed, and dried. The samples were negatively stained for 45 s on 2% uranyl acetate in water. After draining off the excess of staining solution and drying, images were obtained using a ZEISS 912 Omega electron microscope operating at an accelerating voltage of 80 kV.
hIAPP experiments.
Samples were prepared under the same conditions as in the ThT-fluorescence assay. Aliquots of hIAPP (5 µM in 10 mM Tris-HCl, 100 mM NaCl, pH 7.4 in the presence and absence of foldamer **6**) were adsorbed onto 300-mesh carbon grids for 2 min, washed and dried. The samples were negatively stained for 45 s. on 2 % uranyl acetate in water. After draining off the excess of staining solution and drying, the grids were observed using a JEOL 2100HC TEM operating at 200 kV with a LaB6 filament. Images were recorded in zero-loss mode with a Gif Tridiem energy-filtered-CCD camera equipped with a 2k x 2k pixel-sized chip (Gatan inc., Warrendale, PA). Acquisition was accomplished with the Digital Micrograph software (versions 1.83.842, Gatan inc., Warrendale, PA).
Capillary electrophoresis protocol ($A\beta_{1-42}$)
Sample preparation: the commercial $A\beta_{1-42}$ was dissolved upon reception in 0.16% NH_4OH (at 2 mg/mL) for 10 minutes at 20°C, followed by an immediate lyophilization. The dried sample was then stored at -20°C until use.
CE-UV experiments were carried out with a P/ACE ™ MDQ Capillary Electrophoresis System (Beckman Coulter Inc., Brea, CA, USA) equipped with a PDA (photodiode array) detector. UV Detection was performed at 190 nm. The prepared sample (as previously described) was dissolved in 20 mM phosphate buffer at pH 7.4, containing DMSO for control or stock solutions of hexamer **6** to keep constant the DMSO/phosphate buffer ratio at 2.5%. The final peptide concentration was 100 µM with a peptide/compound ratio of 1/1. For the CE separation of Aβ oligomers, it was used a fused silica capillary of 80 cm (10.2 cm to the detector) with an internal diameter of 50 µm. The buffer separation solution was a 80 mM phosphate buffer at pH 7.4. The separation was carried out under -20 kV and constant temperature at 25°C. The samples were injected by hydrodynamic injection at 0.5 psi for 10 s. After each run, the capillary was rinsed for 3.5 min with NaOH 1 M, 3.5 min with water, 1 min with DMSO 10 % and 1 min with SDS 50 mM.

Capillary electrophoresis protocol (hIAPP)
Sample preparation: commercial hIAPP was dissolved upon reception in pure HFIP at 1 mM and incubated for 1 hour at room temperature, followed by an aliquoting and an immediate evaporation under nitrogen, then under vacuum and storage at -20°C. Just before performing real time kinetics, the dried peptide was reconstituted in 50 mM ammonium acetate buffer pH 3.7 at 100 µM. Hexamer **6** was dissolved in DMSO and added to the peptide solution to reach final concentration of 100 µM and DMSO/ammonium acetate buffer ratio of 1%.
CE-UV experiments were carried out with a MDQ Instrument (SCIEX, Fragmingham, MA, USA) equipped with a UV detector. Detection was performed at 200 nm. Fused silica capillaries (50 µm id x 365 µm od) were purchased from Polymicro Technologies (Phoenix, AZ, USA). Silica capillaries were coated with a 0.2% polybrene solution. Briefly, solid polybrene was dissolved in water under heating at 50°C. The capillary was preconditioned with MeOH, NaOH 1M, NaOH 0.1M and with H_2O. All flushings were done at 20 psi for 15 min. The capillary was then coated with the 0.2% polybrene solution for 15 min at 20 psi. The coated capillary was then flushed with the background electrolyte (BGE) at 20 psi for 45 min and equilibrated under -25 kV for 2 hours. Polybrene-

coated capillaries were 60 cm total length (49.8 cm to the detector). The BGE was a 50 mM ammonium acetate buffer, pH 3.7. The separation was carried out under -25 kV at 25°C. Samples were injected from the inlet by hydrodynamic injection at 0.8 psi for 10 s. After each run, the capillary was rinsed for 5 min with 1 M NaOH, 5 min with water, recoated for 10 min with 0.2% polybrene, and finally equilibrated with the running buffer for 5 min at 20 psi.

ESI-MS experiments were carried out with a Synapt G2-S^i Q-TOF instrument (Waters, Manchester, UK) equipped with an ESI interface. Positive ion mode was used. Samples of hIAPP (as previously described for the CE-UV experiments) were injected by direct infusion through a syringe at 5µL/min. Main MS parameters are detailed the following: the capillary voltage was set at 2.4 kV, with the sampling cone and source offset at 70V. Source and dessolvation temperatures were respectively 40 °C and 75°C. Data were processed with MassLynx.

Acknowledgements

IDEX Paris Saclay (IDI 2015, ANR-11-IDEX-0003-02) is acknowledged for financial support of Corentin Berardet (PhD fellowhip). Yasmine Iacone (Erasmus student from the Università degli Studi di Milano) is thanked for her contribution to electrophoresis capillary experiments on $A\beta_{1\text{-}42}$. Ghislaine Frébourg (Institut de Biologie Paris Seine (IBPS)/FR 3631, Service de Microscopie Electronique, Université Pierre et Marie Curie (UPMC), France) is thanked for her contribution to cryo-electron microscopy. The Laboratory BioCIS is a member of the Laboratory of Excellence LERMIT supported by a Grant from ANR (ANR-10-LABX-33). The laboratory PNAS is a member of the Laboratory of Excellence Nanosaclay supported by a Grant from ANR (ANR-10-LABX-0035).

Conflicts of interests

No conflict to declare.

Keywords: amyloid • aggregation • foldamer • peptidomimetic • helix

[1] A. Chaudhury, C. Duvoor, V. S. Reddy Dendi, S. Kraleti, A. Chada, R. Ravilla, A. Marco, N. S. Shekhawat, M. T. Montales, K. Kuriakose, et al., *Front. Endocrinol.* **2017**, *8*, 6.
[2] "World Alzheimer Reports | Alzheimer's Disease International," can be found under https://www.alz.co.uk/research/world-report, **2018**.
[3] C. Messier, *Neurobiol. Aging* **2005**, *26*, 26–30.
[4] J. S. Roriz-Filho, T. M. Sá-Roriz, I. Rosset, A. L. Camozzato, A. C. Santos, M. L. F. Chaves, J. C. Moriguti, M. Roriz-Cruz, *Biochim. Biophys. Acta BBA - Mol. Basis Dis.* **2009**, *1792*, 432–443.
[5] A. Jayaraman, C. J. Pike, *Curr. Diab. Rep.* **2014**, *14*, 476.
[6] M. K. Song, D. S. Bischoff, A. M. Song, K. Uyemura, D. T. Yamaguchi, *BBA Clin.* **2016**, *7*, 41–54.
[7] M. A. Schilling, *J Alzheimers Dis.* **2016**, *51*, 961–977.
[8] D. A. Butterfield, F. Di Domenico, E. Barone, *Biochim. Biophys. Acta* **2014**, *1842*, 1693–1706.
[9] P. C. Ke, M.-A. Sani, F. Ding, A. Kakinen, I. Javed, F. Separovic, T. P. Davis, R. Mezzenga, *Chem. Soc. Rev.* **2017**, *46*, 6492–6531.
[10] R. Riek, D. S. Eisenberg, *Nature* **2016**, *539*, 227–235.
[11] L.-M. Yan, A. Velkova, M. Tatarek-Nossol, E. Andreetto, A. Kapurniotu, *Angew. Chem. Int. Ed. Engl.* **2007**, *46*, 1246–1252.
[12] E. Andreetto, L.-M. Yan, M. Tatarek-Nossol, A. Velkova, R. Frank, A. Kapurniotu, *Angew. Chem. Int. Ed.* **2010**, *49*, 3081–3085.
[13] B. Ren, Y. Liu, Y. Zhang, Y. Cai, X. Gong, Y. Chang, L. Xu, J. Zheng, *ACS Chem. Neurosci.* **2018**, *9*, 1215–1224.
[14] a) F. Belluti, A. Rampa, S. Gobbi, A. Bisi, *Expert Opin. Ther. Pat.* **2013**, *23*, 581–596; b) S.-B. Syarifah-Noratiqah, I. Naina-Mohamed, M. S. Zulfarina, H. M. S. Qodriyah, *Curr Drug Targets* **2018**, *19*, 927–937.
[15] A. Pithadia, J. R. Brender, C. A. Fierke, A. Ramamoorthy, *J. Diabetes Res.* **2016**, 2046327.
[16] S. J. Cox, B. Lam, A. Prasad, H. A. Marietta, N. V. Stander, J. G. Joel, B. R. Sahoo, F. Guo, A. K. Stoddard, M. I. Ivanova, A. Ramamoorthy, bioRxiv 2020, 853499.
[17] I. Benilova, E. Karran, B. De Strooper, *Nat. Neurosci.* **2012**, *15*, 349–357.
[18] L. Haataja, T. Gurlo, C. J. Huang, P. C. Butler, *Endocr. Rev.* **2008**, *29*, 303–316.
[19] Y. Bram, A. Frydman-Marom, I. Yanai, S. Gilead, R. Shaltiel-Karyo, N. Amdursky, E. Gazit, *Sci. Rep.* **2014**, *4*, 4267.
[20] a) D. Goyal, S. Shuaib, S. Mann, B. Goyal, *ACS Comb. Sci.* **2017**, *19*, 55–80; b) V. Armiento, A. Spanopoulou, A. Kapurniotu, *Angew. Chem. Int. Ed.* **2020**, *59*, 3372 – 3384.
[21] S. Pellegrino, N. Tonali, E. Erba, J. Kaffy, M. Taverna, A. Contini, M. Taylor, D. Allsop, M. L. Gelmi, S. Ongeri, *Chem. Sci.* **2017**, *8*, 1295–1302.
[22] N. Tonali, J. Kaffy, J.-L. Soulier, M. L. Gelmi, E. Erba, M. Taverna, C. van Heijenoort, T. Ha-Duong, S. Ongeri, *Eur. J. Med. Chem.* **2018**, *154*, 280–293.
[23] J. Kaffy, D. Brinet, J.-L. Soulier, I. Correia, N. Tonali, K. F. Fera, Y. Iacone, A. R. F. Hoffmann, L. Khemtémourian, B. Crousse, M. Taylor, D. Allsop, M. Taverna, O. Lequin, S. Ongeri, *J. Med. Chem.* **2016**, *59*, 2025–2040.
[24] L. Tran, J. Kaffy, S. Ongeri, T. Ha-Duong, *ACS Chem. Neurosci.* **2018**, *9*, 2859–2869.
[25] C. Nerelius, A. Sandegren, H. Sargsyan, R. Raunak, H. Leijonmarck, U. Chatterjee, A. Fisahn, S. Imarisio, D. A. Lomas, D. C. Crowther, et al., *PNAS* **2009**, *106*, 9191–9196.
[26] L. Fülöp, I. M. Mándity, G. Juhász, V. Szegedi, A. Hetényi, E. Wéber, Z. Bozsó, D. Simon, M. Benkő, Z. Király, et al., *PLoS ONE* **2012**, *7*, e39485.
[27] D. Honcharenko, P. P. Bose, J. Maity, F. R. Kurudenkandy, A. Juneja, E. Flöistrup, H. Biverstål, J. Johansson, L. Nilsson, A. Fisahn, et al., *Org. Biomol. Chem.* **2014**, *12*, 6684–6693.
[28] E. Brandenburg, H. von Berlepsch, U. Gerling, C. Böttcher, B. Koksch, *Chemistry (Weinheim an der Bergstrasse, Germany)* **2011**, *17*, 10651–61.
[29] J.-S. Choi, J. J. Braymer, R. P. R. Nanga, A. Ramamoorthy, M. H. Lim *PNAS* **2010**, *107*, 21990-21995.
[30] S. Kumar, A. Henning-Knechtel, I. Chehade, M. Magzoub, A. D. Hamilton, *J. Am. Chem. Soc.* **2017**, *139*, 17098–17108.
[31] S. Kumar, A. D. Hamilton, *J. Am. Chem. Soc.* **2017**, *139*, 5744–5755.
[32] S. Kumar, M. A. Brown, A. Nath, A. D. Miranker, *Chem. Biol.* **2014**, *21*, 775–781.
[33] S. Kumar, A. D. Miranker, *Chem. Commun.* **2013**, *49*, 4749–4751.
[34] S. Kumar, M. Birol, D. E. Schlamadinger, S. P. Wojcik, E. Rhoades, A. D. Miranker, *Nat. Commun.* **2016**, *7*, 11412.
[35] S. H. Gellman, *Acc. Chem. Res.* **1998**, *31*, 173–180.
[36] S. Hecht, I. Huc, *Foldamers: Structure, Properties and Applications*, Wiley-VCH, Weinheim, **2007**.
[37] G. Guichard, I. Huc, *Chem. Commun.* **2011**, *47*, 5933–5941.
[38] T. A. Martinek, F. Fülöp, *Chem. Soc. Rev.* **2012**, *41*, 687–702.
[39] A. Hassanpour, C. A. De Carufel, S. Bourgault, P. Forgione, *Chem. Eur. J.* **2014**, *20*, 2522–2528.
[40] S. Vivekanandan, J. R. Brender, S. Y. Lee, A. Ramamoorthy, *Biochem. Biophys. Res. Commun.* **2011**, *411*, 312–316.
[41] R. P. R. Nanga, J. R. Brender, S. Vivekanandan, A. Ramamoorthy, *Biochim. Biophys. Acta BBA - Biomembr.* **2011**, *1808*, 2337–2342.
[42] L. Mathieu, B. Legrand, C. Deng, L. Vezenkov, E. Wenger, C. Didierjean, M. Amblard, M.-C. Averlant-Petit, N. Masurier, V. Lisowski, et al., *Angew. Chem. Int. Ed.* **2013**, *52*, 6006–6010.
[43] M. Simon, L. M. A. Ali, K. El Cheikh, J. Aguesseau, M. Gary-Bobo, M. Garcia, A. Morère, L. T. Maillard, *Chem. Eur. J.* **2018**, *24*, 11426–11432.
[44] L. O. Tjernberg, D. J. E. Callaway, A. Tjernberg, S. Hahne, C. Lilliehöök, L. Terenius, J. Thyberg, C. Nordstedt, *J. Biol. Chem.* **1999**, *274*, 12619–12625.
[45] M. Ahmed, J. Davis, D. Aucoin, T. Sato, S. Ahuja, S. Aimoto, J. I. Elliott, W. E. Van Nostrand, S. O. Smith, *Nat. Struct. Mol. Biol.* **2010**, *17*, 561–567.
[46] K. Hochdörffer, J. März-Berberich, L. Nagel-Steger, M. Epple, W. Meyer-Zaika, A. H. C. Horn, H. Sticht, S. Sinha, G. Bitan, T. Schrader, *J. Am. Chem. Soc.* **2011**, *133*, 4348–4358.
[47] C. Wu, J.-E. Shea, *PLoS Comput. Biol.* **2013**, *9*, e1003211.
[48] W. Hoffmann, K. Folmert, J. Moschner, X. Huang, H. von Berlepsch, B. Koksch, M. T. Bowers, G. von Helden, K. Pagel, *J. Am. Chem. Soc.* **2018**, *140*, 244–249.
[49] L. Mathieu, C. Bonnel, N. Masurier, L. T. Maillard, J. Martinez, V. Lisowski, *Eur. J. Org. Chem.* **2015**, *2015*, 2262–2270.
[50] D. Yang, Y.-L. Yan, B. Lui, *J. Org. Chem.* **2002**, *67*, 7429–7431.
[51] C. Bonnel, B. Legrand, J.-L. Bantignies, H. Petitjean, J. Martinez, N. Masurier, L. T. Maillard, *Org. Biomol. Chem.* **2016**, *14*, 8664–8669.
[52] H. LeVine, in *Methods in Enzymology*, Academic Press, **1999**, pp. 274–284.
[53] D. Brinet, J. Kaffy, F. Oukacine, S. Glumm, S. Ongeri, M. Taverna, *Electrophoresis* **2014**, *35*, 3302–3309.
[54] C. Berardet, J. Kaffy, S. Ongeri, M. Taverna, *J. of Chromatogr. A* **2018**, *1578*, 83–90.
[55] C. Berardet, J. Kaffy, F. Halgand, G. Van der Rest, S. Ongeri, M. Taverna, *Anal. Bioanal. Chem.* **2020**,*412*, 3103-3111.
[56] L. M. Young, P. Cao, D. P. Raleigh, A. E. Ashcroft, S. E. Radford, *J. Am. Chem. Soc.* **2014**, *136*, 660–670.
[57] L. M. Young, J. C. Saunders, R. A. Mahood, C. H. Revill, R. J. Foster, L.-H. Tu, D. P. Raleigh, S. E. Radford, A. E. Ashcroft, *Nat. Chem.* **2015**, *7*, 73–81.
[58] L. M. Young, J. C. Saunders, R. A. Mahood, C. H. Revill, R. J. Foster, A. E. Ashcroft, S. E. Radford, *Methods San Diego Calif* **2016**, *95*, 62–69.
[59] I. Riba, P. E. Barran, G. J. S. Cooper, R. D. Unwin, *Int. J. Mass Spectrom.* **2015**, *391*, 47–53.
[60] H. Li, E. Ha, R. P. Donaldson, A. M. Jeremic, A. Vertes, *Anal. Chem.* **2015**, *87*, 9829–9837.

Entry for the Table of Contents

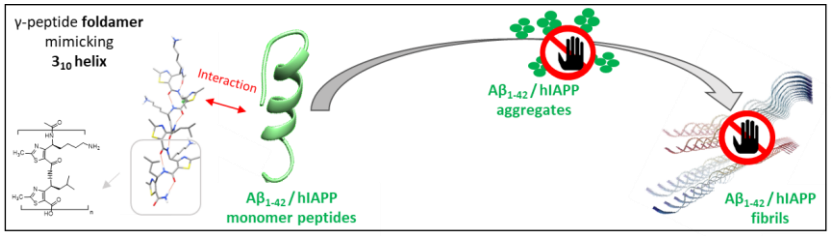

Helical foldamers based on six units of 4-amino(methyl)-1,3-thiazole-5-carboxylic acid (ATC) trap the non-toxic monomeric species of $A\beta_{1-42}$ and hIAPP amyloid peptides, involved in Alzheimer's disease and Type 2 Diabetes respectively.

Institute and/or researcher Twitter usernames:
@UnivParisSaclay
@BioCIS